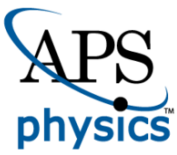

Validating first-principles phonon lifetimes via inelastic neutron scattering

Enda Xiao, Hao Ma, Matthew S. Bryan, Lyuwen Fu, J. Matthew Mann, Barry Winn, Douglas L. Abernathy, Raphaël P. Hermann, Amey R. Khanolkar, Cody A. Dennett, David H. Hurley, Michael E. Manley, and Chris A. Marianetti

Phys. Rev. B **106**, 144310 — Published 24 October 2022

DOI: 10.1103/PhysRevB.106.144310

Validating First-Principles Phonon Lifetimes via Inelastic Neutron Scattering

Enda Xiao[1], Hao Ma[2], Matthew S. Bryan[2], Lyuwen Fu[3], J. Matthew Mann[4], Barry Winn[5], Douglas L. Abernathy[5], Raphaël P. Hermann[2], Amey R. Khanolkar[6], Cody A. Dennett[6], David H. Hurley[6], Michael E. Manley[2], Chris A. Marianetti[3]

[1]*Department of Chemistry, Columbia University, New York, New York 10027, USA*

[2]*Materials Science and Technology Division, Oak Ridge National Laboratory, Oak Ridge, Tennessee 37831, USA*

[3]*Department of Applied Physics and Applied Mathematics, Columbia University, New York, New York 10027, USA*

[4]*Air Force Research Laboratory, Sensors Directorate, Wright-Patterson AFB, OH 45433, USA*

[5]*Neutron Scattering Division, Oak Ridge National Laboratory, Oak Ridge, Tennessee 37831, USA and*

[6]*Materials Science and Engineering Department, Idaho National Laboratory, Idaho Falls, ID 83415, USA*

(Dated: August 4, 2022)

Phonon lifetimes are a key component of quasiparticle theories of transport, yet first-principles lifetimes are rarely directly compared to inelastic neutron scattering (INS) results. Existing comparisons show discrepancies even at temperatures where perturbation theory is expected to be reliable. In this work, we demonstrate that the reciprocal space voxel (q-voxel), which is the finite region in reciprocal space required in INS data analysis, must be explicitly accounted for within theory in order to draw a meaningful comparison. We demonstrate accurate predictions of peak widths of the scattering function when accounting for the q-voxel in CaF_2 and ThO_2. Passing this test implies high fidelity of the phonon interactions and the approximations used to compute the Green's function, serving as critical benchmark of theory, and indicating that other material properties should be accurately predicted; which we demonstrate for thermal conductivity.

When computing anharmonic vibrational properties from first-principles, various approximations are employed, making it challenging to assess the integrity of any single observable as compared to experiment (e.g. thermal conductivity). Comparing a q-space resolved observable (e.g. the scattering function) inherently provides a large number of comparisons, offering a very stringent test. While verification of the harmonic vibrational first-principles Hamiltonian is a standard practice, the same cannot be said for the anharmonic vibrational Hamiltonian and subsequent approximations which are used to compute observables. Anharmonic terms result in finite phonon lifetimes yielding finite widths of the peaks in the scattering function. A direct comparison of peak width between theory and INS is rare, and existing studies reveal anomalous discrepancies. A recent study on Si notes the large discrepancy between theory and experiment, leading the authors to only compare the relative change as a function of temperature[1]. A study on Al at high temperatures finds that perturbation theory does not reliably predict the experimental peak width, and their first-principles molecular dynamics simulations often differ from experiment by a factor of two[2].

Here we show that a proper comparison between the theoretical and experimental scattering function requires an explicit accounting for the finite region probed in reciprocal space, which is referred to as the q-voxel. Due to the flux-limited nature of INS, there is a minimum region of q-space which can be sampled while maintaining sufficient statistics, and therefore there is a minimum q-voxel size below which INS cannot probe. Depending on the measurement type, the q-voxel shape is either set by the instrument configuration (for triple-axis) or defined post measurement in the analysis of large volumes of data (for time-of-flight). This work will focus on the latter since the large data volumes allow for a more comprehensive assessment across many zones and with varying q-voxels. While there is no formal standard for choosing a q-voxel, it is typical to choose the q-voxel size and shape based on the shape of the phonon dispersion surface; selecting a smaller dimension along directions with steeper dispersion and larger dimensions along directions with flatter dispersion.

In the present work, we demonstrate the critical role of the q-voxel using two fluorite structured materials, ThO_2 and CaF_2, showing excellent agreement between peakwidths within a q-voxel obtained from INS and computed from perturbation theory based on the first-principles phonons and cubic phonon interactions. Successful agreement validates both the anhmarmonic Hamiltonian and the level of theory being used to evaluate the scattering function. Given our successful peakwidth predictions, it is expected that thermal conductivity predicted using the same anhmarmonic Hamiltonian and the Boltzmann transport equation should faithfully describe experimental measurements in some temperature regime, which is demonstrated for CaF_2 and ThO_2.

Time-of-flight INS measurements were performed using the ARCS[3] and HYSPEC[4] instruments at the Spallation Neutron Source. Thermal conductivity measurements were made on single crystal ThO_2 using spatial domain thermoreflectance (SDTR) via the methods described in [5]. First-principles calculations were performed using density functional theory (DFT) with the

strongly constrained and appropriately normed (SCAN) functional[6], and phonons and cubic phonon interactions were computed using the lone and bundled irreducible derivative approaches[7, 8]. Detailed information about experimental and computational methods are included in supplemental material [8].

In order to compute the phonon linewidths and the one-phonon scattering function $S_1(\mathbf{Q},\omega)$, the single-particle phonon Green's function can be approximately evaluated using the phonons and cubic phonon interactions within leading order perturbation theory[9, 10] (see Eq. 2 in [8]). The scattering function $S_1(\mathbf{Q},\omega)$ is evaluated precisely at $\mathbf{Q}$, but in INS experiments a finite q-voxel must be chosen to provide sufficient counting statistics. This q-voxel can be accounted for theoretically by integrating $S_1(\mathbf{Q},\omega)$ over the q-voxel, resulting in

$$S_1^{\text{vox}}(\mathbf{Q},\omega) = \frac{1}{\Omega_{\text{vox}}} \int_{\text{vox}} d^3Q' \;\; S_1(\mathbf{Q}',\omega), \qquad (1)$$

where Ω_{vox} is the reciprocal space volume of the q-voxel. For clarity, we refer to $S_1(\mathbf{Q},\omega)$ as the q-point scattering function and $S_1^{\text{vox}}(\mathbf{Q},\omega)$ as the q-voxel scattering function. It should be noted that the widths of $S_1^{\text{vox}}(\mathbf{Q},\omega)$ can vary from zone to zone, unlike $S_1(\mathbf{Q},\omega)$ [8].

We now proceed to evaluate the q-point and q-voxel scattering function in CaF_2 and ThO_2, and compare them to INS measurements. Given that CaF_2 and ThO_2 are band insulators, standard implementations of DFT are expected to perform well in terms of describing the ground state properties. As anticipated, the computed phonon spectrum is in good agreement with the scattering function peak positions obtained from INS at ambient temperature for both CaF_2 (see Fig. 1, panel *a*) and ThO_2 (see Fig. S2 in [8]). While the peak locations agree well, it is interesting to directly compare the respective scattering functions via contour plots along a path through q-space (see Fig.1, panel *b*). For a direct comparison, the INS instrumental energy resolution is accounted for in the theoretical result[3]. We find that the theoretical and INS q-voxel scattering functions are in reasonable agreement, while they have nontrivial differences with the q-point scattering function in certain regions. The theoretical q-voxel scattering function even recovers subtle features of the INS, such as the presence of the TA1 band (see panel *a* for naming convention), which is forbidden in the q-point scattering function for the path shown, but is visible in the q-voxel scattering function [11]. In order to illustrate potential differences between the q-point and q-voxel scattering function, both large and small, we present the scattering function at two Q points as a function of energy around the LO1 band, which scatters strongly (see Fig.1, panels *c* and *d*). As shown, the Q which is closer to the zone center (panel *d*) only shows negligible differences between the q-point and q-voxel scattering functions, while the other Q (panel *c*)

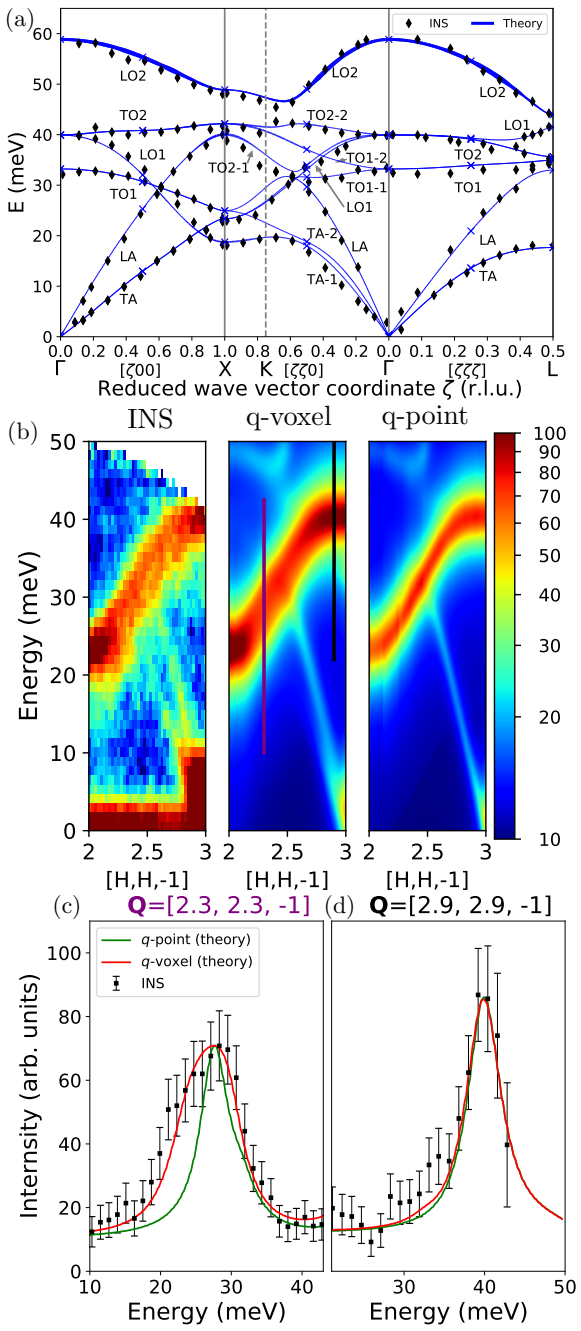

FIG. 1. (a) Phonon dispersion of CaF_2. Black points are INS measurements at $T = 300$K; blue crosses are computed using DFT (SCAN), blue lines are a Fourier interpolation, and the line width is proportional to the computed phonon linewidth. (b) Color contour plots of the scattering function as a function of energy and $\mathbf{Q}$ obtained using INS, theoretical q-voxel, and theoretical q-point results. The q-voxel dimensions are 0.025 r.l.u. along the [H,H,0] direction (i.e. the dispersion direction) and relaxed to 0.2 r.l.u along the orthogonal directions [0,0,L] and [H,-H,0]. (c, d) Scattering function as a function of energy at selected Q-points, corresponding to purple and black lines in the color contour plots. The red and green curves are theoretical q-voxel and q-point scattering functions, respectively; black points are INS measurements.

shows good agreement between the theoretical and experimental q-voxel scattering function, but a substantial difference with the q-point scattering function; and this difference may be attributed to the large slope in the latter case. The preceding examples already illustrate that one can only meaningfully compare theory and experiment if q-voxel quantities are being employed.

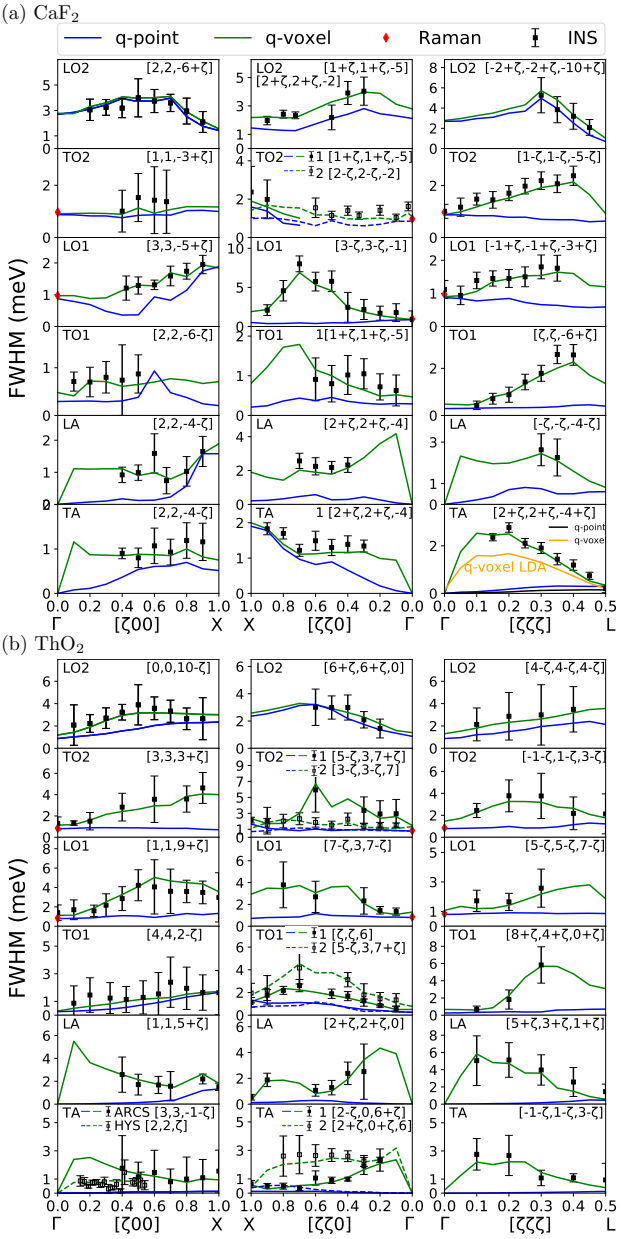

FIG. 2. FWHM's of the scattering function peaks as a function of q in various zones for CaF_2 (panel a) and ThO_2 (panel b) at $T = 300$ K. The DFT (SCAN) q-point and q-voxel results are shown as blue and green lines, respectively; INS results are shown as black points. Certain panels contain multiple modes (see legend). The q-voxel dimensions are reported in supplemental material[8]. Previous Raman measurements are denoted by a red diamond[12, 13].

Having illustrated that accounting for the q-voxel scattering function can be critical to describing experiments, we now proceed to comprehensively quantify the differences across the Brillouin zone for both CaF_2 and ThO_2. In Fig.2, we compare the full width at half maximum (FWHM) of each peak obtained from the INS q-voxel scattering function, the theoretical q-voxel scattering function, and the theoretical q-point scattering function (see [8] for **Q** and voxel sizes). Following standard INS conventions, the energy resolution is removed from the INS scattering function peak width[3, 14]. The INS and theoretical q-voxel FWHM results are in favorable agreement across all modes and q-paths, while there is substantial difference with the FWHM obtained from the theoretical q-point scattering function in most cases. The acoustic modes, which are highly relevant for thermal conductivity, show a strong difference between q-voxel and q-point FWHM values. We also compare our theoretical results at the Γ point to the Raman measurements of the T_{2g} widths in CaF_2 [12] and ThO_2 [13], indicated with a red diamond, demonstrating good agreement with the q-point result; which is to be expected. In summary, we have shown that it is critical to employ the q-voxel in order to validate a first-principles theory using INS.

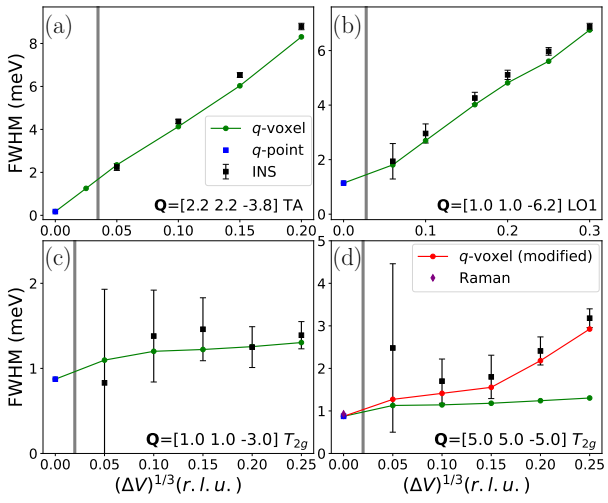

FIG. 3. The FWHM as a function of the cubic q-voxel dimension in CaF_2 at $T = 300$ K for three modes: the TA mode at **Q** =[2.2, 2.2, -3.8] (panel a), the LO1 mode at **Q** =[1.0, 1.0, -6.2] (panel b), and the T_{2g} mode at **Q** =[1.0, 1.0, -3.0] (panel c) and **Q** =[5.0, 5.0, -5.0] (panel d). See text for explanation of q-voxel (modified) result (red line). The q-resolution of the instrument is shown by a gray vertical line. The Raman measurement of the T_{2g} width in CaF_2 by Elliott *et al.*[12] is shown as a purple diamond.

In the preceding analysis, we demonstrated that theory and experiment are in good agreement when using the same q-voxel, and that the results can be substantially different from the q-point results. Now we explore the effect of voxel size in the case of a cubic voxel, and examine

the possibility of extrapolating the q-voxel results to zero voxel size in order to recover the q-point results, which would allow INS experiments to independently obtain q-point peakwidths. The q-voxel size used in INS data analysis is a compromise between having good counting statistics (larger volume) and minimizing contamination from neighboring regions in reciprocal space (smaller volume). The minimum possible INS q-voxel size will be set by the instrument q-resolution, though this is normally far too small to obtain sufficient counting statistics. The effects of the q-voxel size on the experimental FWHM of CaF_2 is shown in Fig.3 for three different modes: the TA mode at $\mathbf{Q}$ =[2.2, 2.2, -3.8], the LO1 mode at $\mathbf{Q}$ =[1.0, 1.0, -6.2], and the T_{2g} mode (i.e. LO1+TO2) at $\mathbf{Q}$ =[1.0, 1.0, -3.0] and $\mathbf{Q}$ =[5.0, 5.0, -5.0]. With the exception of the T_{2g} mode at $\mathbf{Q}$ =[5.0, 5.0, -5.0] (i.e. Fig.3, panel d), the theoretical results are in good agreement with experiment for a sufficiently large voxel size; and the exception can be attributed to the overlap of the T_{2g} peak with the TO1 peak, which corrupts the fitting process for the experimental data which must account for the energy resolution of the instrument. To make a direct comparison, we convolve the theoretical results with the energy resolution, and then perform the identical fitting process used for the experimental results where the energy resolution is removed (see red line in Fig.3, panel d). This modified theoretical result now agrees well with experiment for large q-voxel sizes, and recovers the usual theoretical q-voxel results at small q-voxel sizes. Our analysis resolves a previous anomoly in the literature, explaining why the INS peak width of the T_{2g} mode was found to be more than twice that of Raman measurements[15]. Nonetheless, the simplest solution to this problem is to choose a more favorable zone, as shown in Fig.3, panel c. In all the preceding examples, we see that sufficiently small voxel sizes lead to poor results for the experimental case given the poor counting statistics, as expected. Furthermore, it appears that there is sufficient uncertainty within the experimental measurements which would preclude the possibility of extrapolating to zero voxel size to obtain the peakwidth purely from experiment. The effects on non-cubic voxels are explored in Supplementary Material[8] (see Section VII).

We have demonstrated that the q-voxel peakwidths from theory and experiment are in good agreement at room temperature. This agreement serves as a verification of the quality of our cubic phonon interactions, in addition to the level of perturbation theory used to construct the scattering function. The former is an indirect assessment of the quality of the approximation to the exchange-correlation energy used within DFT, and it should be emphasized that the SCAN functional is critical to such good agreement; whereas the local density approximation [21] (LDA) produces substantial deviations (see Fig. 3, panel a, orange line, and [8], Section VIII). We can now predict other quantities, such as thermal conductivity, and anticipate robust results. The thermal conductivity can be computed by solving the linearized Boltzmann transport equation (LBTE) [22–24]. Within the relaxation time approximation (RTA), the LBTE solution is obtained as an explicit function of the phonon spectrum and the phonon linewidths. The RTA is sometimes an excellent approximation to the LBTE solution, and previous work has demonstrated that this is the case in CaF_2 [25]; and we reach the same conclusion in both CaF_2 and ThO_2. Therefore, we expect our predicted thermal conductivity to be very robust, and we evaluate both CaF_2 and ThO_2.

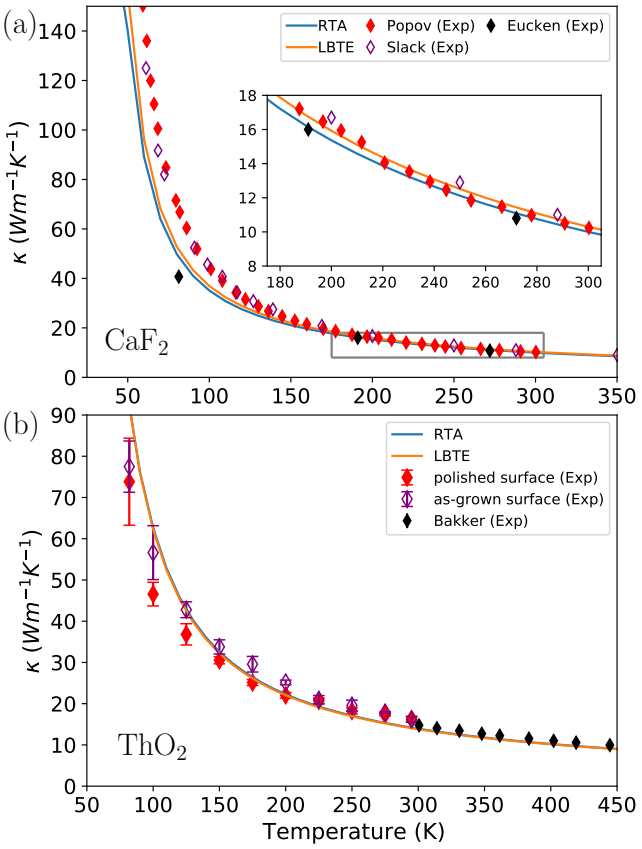

FIG. 4. Thermal conductivity κ as a function of temperature in CaF_2 (panel a) and ThO_2 (panel b). Our DFT (SCAN) results are denoted with orange and blue lines for LBTE and RTA solutions, respectively. Experimental measurements on CaF_2 by Slack[16], Eucken[17], and Popov *et al.*[18, 19] are shown, in addition to measurements in ThO_2 by Bakker *et al.*[20] and our own (with one sample having a polished surface [8]).

In the case of CaF_2 (Fig.4, panel a), our predictions are in good agreement with all available experimental data [16–18] in the temperature range of 200 K to 300 K. At low temperatures, the results of both Slack[16] and Popov *et al.* [18] are somewhat higher than our predictions, though the single measurement at $T = 77K$ by Eucken[17] is below our result. In the case of ThO_2

(Fig.4, panel *b*), our predicted thermal conductivity is in good agreement with the data of Bakker *et al.* [20], which extends from 300 K to 450 K, and reasonable comparison is found with our measurements from 82 K to 295 K. The higher conductivity predicted at low temperatures as compared with our experiments may be due to small, native impurity concentrations resulting from the hydrothermal growth process. Our laser based measurements show nontrivial variability at low temperatures based on the surface condition of the sample, and there is a small difference with the data of Bakker *et al.* near room temperature. It is difficult to assess which experimental results are more reliable. Comparison with previous first-principles calculations is provided in Supplementary Material for both CaF_2 and ThO_2 [8].

In summary, we have shown that the q-voxel of the INS measured scattering function must be accounted for when comparing to theoretical predictions, elucidating why INS peak widths had not been well matched to predictions until now. Given that the q-voxel can be straightforwardly implemented within theory, INS is thus elevated to a refined judge of all ingredients of a quasiparticle theory of phonons, whether ab-initio or empirical. The q-voxel should be carefully considered in the design of future INS instruments, with the possible goal of allowing INS to independently extrapolate to the q-point limit.

ACKNOWLEDGEMENT

INS measurements by M.S.B., H. M., and M.E.M., first-principles calculations by E.X., L.F., and C.A.M., crystal growth by J.M.M., and thermal conductivity measurements by C.A.D., A.R.K., and D.H.H. were supported by the Center for Thermal Energy Transport under Irradiation, an Energy Frontier Research Center funded by the U.S. Department of Energy (DOE), Office of Science, United States, Office of Basic Energy Sciences. Neutron scattering data acquisition and provision of CaF2 by R.P.H. was supported by the DOE Office of Science, Basic Energy Science, Materials Science and Engineering Division. Portions of this research used resources at the Spallation Neutron Source, a U.S. DOE Office of Science User Facility operated by the Oak Ridge National Laboratory. This research used resources of the National Energy Research Scientific Computing Center, a DOE Office of Science User Facility supported by the Office of Science of the U.S. Department of Energy under Contract No. DE-AC02-05CH11231. The formulation and encoding of linewidths via irreducible derivatives by L.F. and C.A.M. was supported by the grant DE-SC0016507 funded by the U.S. Department of Energy, Office of Science.

*E.X., H.M. and M.S.B. contributed equally to this work.

[1] D. S. Kim, O. Hellman, N. Shulumba, C. N. Saunders, J. Y. Lin, H. L. Smith, J. Herriman, J. L. Niedziela, D. L. Abernathy, C. W. Li, *et al.*, Physical Review B **102**, 174311 (2020).

[2] A. Glensk, B. Grabowski, T. Hickel, J. Neugebauer, J. Neuhaus, K. Hradil, W. Petry, and M. Leitner, Physical review letters **123**, 235501 (2019).

[3] D. L. Abernathy, M. B. Stone, M. Loguillo, M. Lucas, O. Delaire, X. Tang, J. Lin, and B. Fultz, Review of Scientific Instruments **83**, 015114 (2012).

[4] S. Shapiro, I. Zaliznyak, L. Passell, V. Ghosh, W. Leonhardt, and M. Hagen, Physica B: Condensed Matter **385**, 1107 (2006).

[5] C. A. Dennett, W. R. Deskins, M. Khafizov, Z. Hua, A. Khanolkar, K. Bawane, L. Fu, J. M. Mann, C. A. Marianetti, L. He, D. H. Hurley, and A. El-Azab, Acta Mater. **213**, 116934 (2021).

[6] J. Sun, A. Ruzsinszky, and J. Perdew, Phys. Rev. Lett. **115**, 036402 (2015).

[7] L. Fu, M. Kornbluth, Z. Cheng, and C. A. Marianetti, Phys. Rev. B **100**, 014303 (2019).

[8] See Supplemental Material at [URL will be inserted by publisher] for details of sample prepatation, INS information, and details of DFT calculations. Refs. [3–7, 10, 14, 18, 19, 21, 25–39] are cited.

[9] J. J. Kokkedee, Physica **28**, 374 (1962).

[10] A. Maradudin and A. Fein, Physical Review **128**, 2589 (1962).

[11] G. Shirane, S. M. Shapiro, and J. M. Tranquada, *Neutron Scattering with a Triple-Axis Spectrometer: Basic Techniques* (Cambridge University Press, Cambridge, 2002).

[12] R. J. Elliott, W. Hayes, W. G. Kleppmann, A. J. Rushworth, and J. F. Ryan, Proceedings of the Royal Society of London. A. Mathematical and Physical Sciences **360**, 317 (1978).

[13] R. Rao, R. Bhagat, N. P. Salke, and A. Kumar, Appl Spectrosc **68**, 44 (2014).

[14] S. D. Bruce, J. Higinbotham, I. Marshall, and P. H. Beswick, Journal of Magnetic Resonance **142**, 57 (2000).

[15] K. Schmalzl, D. Strauch, and H. Schober, Physical Review B **68**, 144301 (2003).

[16] G. A. Slack, Phys. Rev. **122**, 1451 (1961).

[17] A. Eucken, Annalen der Physik **339**, 185 (1911).

[18] P. A. Popov, P. P. Fedorov, and V. V. Osiko, Dokl. Phys. **59**, 199 (2014).

[19] The experimental data of Popov et. al[18] was digitized incorrectly by Qi et. al[25].

[20] K. Bakker and E. H. P. Cordfunke, , 12.

[21] J. P. Perdew and A. Zunger, Phys. Rev. B **23**, 5048 (1981).

[22] D. A. Broido, A. Ward, and N. Mingo, Phys. Rev. B **72**, 014308 (2005).

[23] D. A. Broido, L. Lindsay, and A. Ward, Phys. Rev. B **86**, 115203 (2012).

[24] L. Chaput, Phys. Rev. Lett. **110**, 265506 (2013).

[25] Y.-Y. Qi, T. Zhang, Y. Cheng, X.-R. Chen, D.-Q. Wei, and L.-C. Cai, Journal of Applied Physics **119**, 095103 (2016).

[26] M. Mann, D. Thompson, K. Serivalsatit, T. M. Tritt, J. Ballato, and J. Kolis, Crystal growth & design **10**, 2146 (2010).

[27] M. S. Bryan, L. Fu, K. Rickert, D. Turner, T. A. Prusnick, J. M. Mann, D. L. Abernathy, C. A. Marianetti, and M. E. Manley, Communications Physics **3**, 1 (2020).

[28] J. Y. Lin, A. Banerjee, F. Islam, M. D. Le, and D. L. Abernathy, Physica B: Condensed Matter **562**, 26 (2019).

[29] M. B. Stone, J. L. Niedziela, D. L. Abernathy, L. DeBeer-Schmitt, G. Ehlers, O. Garlea, G. E. Granroth, M. Graves-Brook, A. I. Kolesnikov, A. Podlesnyak, and B. Winn, Review of Scientific Instruments **85**, 045113 (2014), publisher: American Institute of Physics.

[30] C. A. Dennett, Z. Hua, A. Khanolkar, T. Yao, P. K. Morgan, T. A. Prusnick, N. Poudel, A. French, K. Gofryk, L. He, L. Shao, M. Khafizov, D. B. Turner, J. M. Mann, and D. H. Hurley, APL Mater. **8**, 111103 (2020).

[31] P. E. Blöchl, O. Jepsen, and O. K. Andersen, Phys. Rev. B **49**, 16223 (1994).

[32] G. Kresse and D. Joubert, Phys. Rev. B **59**, 1758 (1999).

[33] A. C. Momin, E. B. Mirza, and M. D. Mathews, Journal of Nuclear Materials **185**, 308 (1991).

[34] B. Schumann and H. Neumann, Crystal Research and Technology **19**, K13 (1984).

[35] H. Nakamura and M. Machida, Journal of Nuclear Materials **519**, 45 (2019).

[36] R. Bader, M. Brehm, R. Ebner, H. Heller, L. Palm, and F. Wagner, *High Performance Computing in Science and Engineering, Munich 2002*, edited by S. Wagner, A. Bode, W. Hanke, and F. Durst (Springer, Berlin, Heidelberg, 2003).

[37] R. M. Hazen and L. W. Finger, Journal of Applied Crystallography **14**, 234 (1981).

[38] O. Arnold, J. Bilheux, J. Borreguero, A. Buts, S. Campbell, L. Chapon, M. Doucet, N. Draper, R. Ferraz Leal, M. Gigg, V. Lynch, A. Markvardsen, D. Mikkelson, R. Mikkelson, R. Miller, K. Palmen, P. Parker, G. Passos, T. Perring, P. Peterson, S. Ren, M. Reuter, A. Savici, J. Taylor, R. Taylor, R. Tolchenov, W. Zhou, and J. Zikovsky, Nuclear Instruments and Methods in Physics Research Section A: Accelerators, Spectrometers, Detectors and Associated Equipment **764**, 156 (2014).

[39] F. Akeroyd, S. Ansell, S. Antony, O. Arnold, A. Bekasovs, J. Bilheux, J. Borreguero, K. Brown, A. Buts, S. Campbell, D. Champion, L. Chapon, M. Clarke, S. Cottrell, R. Dalgliesh, D. Dillow, M. Doucet, N. Draper, R. Fowler, M. A. Gigg, G. Granroth, M. Hagen, W. Heller, A. Hillier, S. Howells, S. Jackson, D. Kachere, M. Koennecke, C. Le Bourlot, R. Leal, V. Lynch, P. Manuel, A. Markvardsen, R. McGreevy, D. Mikkelson, R. Mikkelson, R. Miller, S. Nagella, T. Nielsen, K. Palmen, P. G. Parker, M. Pascal, G. Passos, T. Perring, P. F. Peterson, F. Pratt, T. Proffen, P. Radaelli, J. Rainey, S. Ren, M. Reuter, L. Sastry, A. Savici, J. Taylor, R. J. Taylor, M. Thomas, R. Tolchenov, R. Whitley, M. Whitty, S. Williams, W. Zhou, and J. Zikovsky, Mantid: Manipulation and Analysis Toolkit for Instrument Data. (2013), language: en.